RSC Advances

PAPER

View Article Online
View Journal | View Issue

Cite this: *RSC Adv.*, 2025, **15**, 38176

Thymoquinone chemically conjugated to doxorubicin: antitumor activity and subcellular localization

Ismail Sami Mahmoud, *[a] Hamdi Nsairat,*[b] Shorouq Alsotari,[c] Areej Jaber, [b] Ezaldeen Esawi, [d] Hiba Abdelnabi,[c] Majed Al Holi,[c] El Soubani Fatima,[e] Walhan Alshaer [bc] and Fadwa Odeh [f]

Doxorubicin is a chemotherapeutic agent that is frequently used in the treatment of several cancers including breast, lung, gastric, ovarian, and thyroid cancers and lymphoma. Despite the wide use of doxorubicin in cancer treatment, the drug has demonstrated severe side effects such as cardiotoxicity, bone marrow aplasia and nephrotoxicity. On the other hand, thymoquinone is a phytochemical antioxidant with known chemopreventive and chemotherapeutic activities. However, thymoquinone suffers from high hydrophobicity, causing poor solubility in aqueous medium, which limits its bioavailability. In this study, we developed a new strategy to attenuate doxorubicin-induced toxicity and improve the bioavailability of thymoquinone by a direct chemical conjugation between doxorubicin and thymoquinone. Strikingly, the generated hybrid drug of thymoquinone-doxorubicin showed a high anti-tumor efficacy, particularly against the MCF-7 breast cancer cells, and low toxicity towards normal human cells. This indicated the potential use of this hybrid drug to target cancer cells with high efficiency and low side toxicity. Moreover, the subcellular localization of the hybrid drug was identified using confocal laser scanning microscopy and fluorescence live-cell imaging, and it was found to be predominantly localized to the endoplasmic reticulum of the cells.

Received 29th July 2025
Accepted 23rd September 2025

DOI: 10.1039/d5ra05492c

rsc.li/rsc-advances

1 Introduction

Cancer is a public health problem and continues to be among the leading causes of morbidity and mortality worldwide. Generally, a cancer cell is characterized by its six main capabilities: sustaining proliferative signaling, evading growth suppressors, activating metastasis, enabling immortal replication, promoting angiogenesis and resisting apoptosis.[1] Anti-cancer agents like those used in chemotherapies have been developed to destroy cancer cells by stopping or slowing the capabilities of cancer cells, and they are considered a primary treatment technique for treating millions of cancer patients worldwide.[2] Doxorubicin (Dox, Fig. 1A) is one of the most commonly used chemotherapeutic drugs for treating a wide range of cancers, including breast, lung, and bladder cancers, lymphoma and leukaemia.[3–5] Its primary function is to suppress topoisomerase I and II and intercalate into DNA to interfere with its uncoiling, ultimately inducing cell death.[3] Another mechanism is the generation of free radicals, which, in turn, can damage DNA and biomolecules and result in cell death.[6] However, Dox does not specifically target cancer cells, and it will also eliminate normal healthy cells, especially those that frequently divide.[3] As multiple tissues are destroyed, organ toxicity occurs. Indeed, clinical studies show that the heart is a primary target of Dox-induced side toxicity.[7] However, Dox toxicity could also affect other organs, such as the brain, bone marrow, kidney and liver.[8]

Thymoquinone (TQ, Fig. 1B) is the main bioactive constituent of the volatile oil of the black seed (*Nigella sativa*, Ranunculaceae family), and it has been shown to exhibit anti-cancerous, antioxidant and anti-inflammatory activities both *in vitro* and *in vivo*.[9–11] The antioxidant activity of TQ has been extensively studied. Indeed, TQ was reported to decrease liver toxicity in mice treated with Aflatoxin B(1).[12] TQ pretreatment was able to reduce the levels of AST, ALT and ALP liver enzymes after administration of Aflatoxin B(1), and it prevented the formation of the reactive aldehyde malondialdehyde (MDA), the end product of lipid peroxidation in the liver.[12] In addition, the researchers showed that pretreatment with TQ significantly restored the hepatic supply of glutathione in mice compared to

[a]*Department of Medical Laboratory Sciences, Faculty of Applied Medical Sciences, The Hashemite University, Zarqa 13133, Jordan. E-mail: ismails@hu.edu.jo; Tel: +962797545880*

[b]*Pharmacological and Diagnostic Research Center, Faculty of Pharmacy, Al-Ahliyya Amman University, Amman 19328, Jordan. E-mail: h.alnseirat@ammanu.edu.jo; Tel: +962796167327*

[c]*Cell Therapy Centre, The University of Jordan, Amman 11942, Jordan*

[d]*South Australian ImmunoGENomics Cancer Institute, University of Adelaide, Adelaide, SA 5000, Australia*

[e]*Department of Chemistry, The Hashemite University, Zarqa 13133, Jordan*

[f]*Department of Chemistry, The University of Jordan, Amman, Jordan*

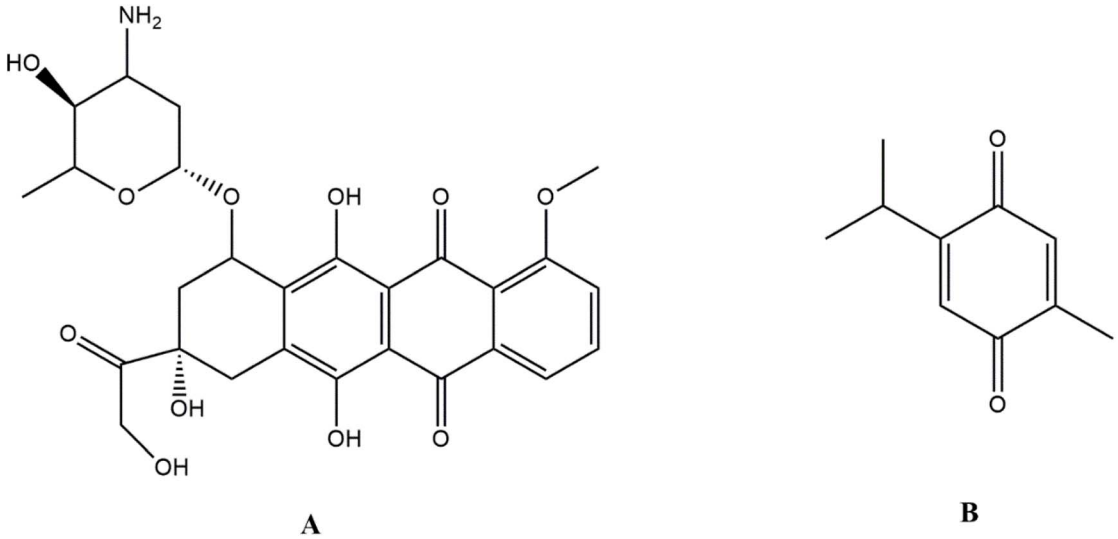

Fig. 1 Chemical structures of (A) doxorubicin (Dox) and (B) thymoquinone (TQ).

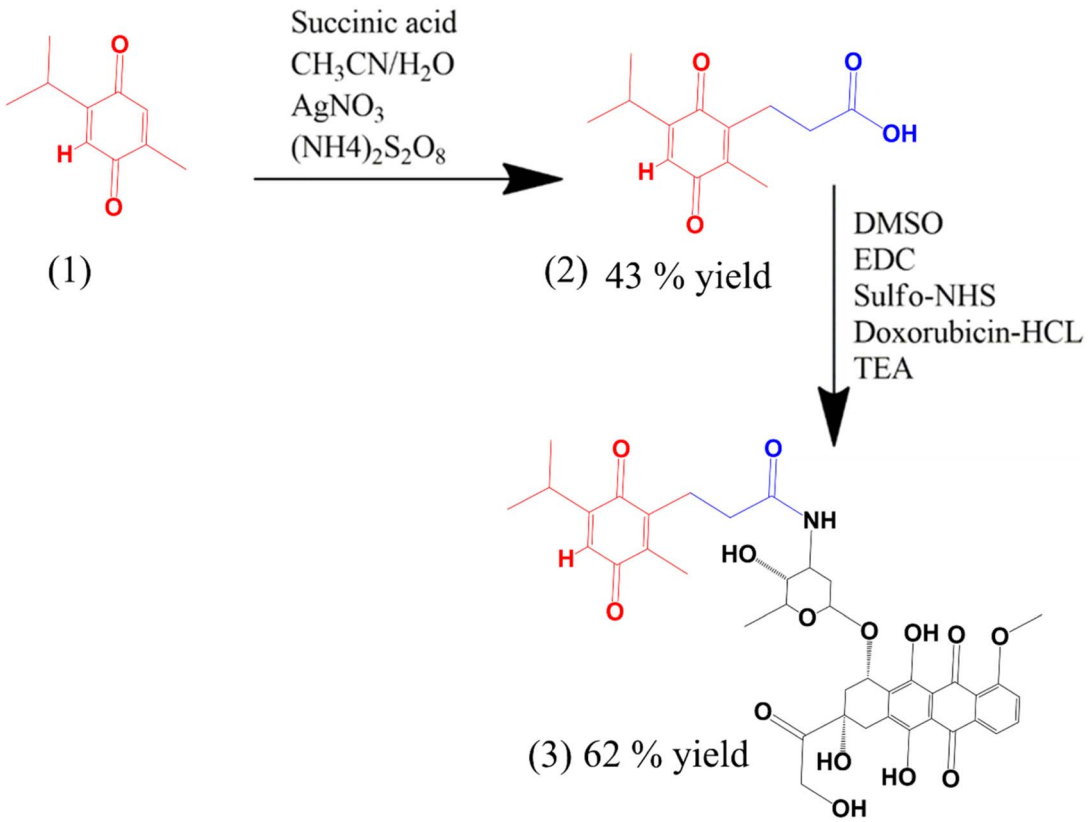

Fig. 2 Chemical conjugation strategy of the hybrid drug (TQ-Suc-Dox). A chemical reaction for the conjugation of TQ (1) with the linker succinic acid (Suc) to produce TQ-Suc (2) was conducted by transferring a specific amount of TQ and succinic acid to a 25 mL two-neck flask. Then, the chemicals were dissolved in a mixture (9 mL total volume) of (1 : 1) acetonitrile (CH_3CN):water, under an inert atmosphere (argon gas). Directly, silver nitrate ($AgNO_3$) was added, and the mixture was left for 2–3 min at RT under argon gas. Then, the reaction mixture was heated to 80 °C with reflux (5 min). After that, ammonium persulfate $(NH_4)_2S_2O_8$ was added gradually. The reaction mixture was refluxed at 100 °C overnight. Then, diethyl ether was used as an extraction solvent for extraction. The organic layer was taken and dried over anhydrous sodium sulfate (Na_2SO_4) powder and evaporated at atmospheric pressure overnight. For chemical conjugation of TQ-Suc with Dox to produce the hybrid compound TQ-Suc-Dox (3), TQ-Suc was dissolved in DMSO and stirred under nitrogen gas. To activate the carboxylic acid group, EDC was added to the TQ-Suc acid solution, followed by Sulfo-NHS, and the mixture was stirred for 3 hours. Dox-HCL dissolved in DMSO with trace amounts of triethylamine was then added to the reaction solution, with magnetic stirring for 12–24 hours in dark under nitrogen.

the untreated group.[12] Also, TQ was found to reverse the symptoms of myocardial injury (MI) and restore the levels of glutathione and superoxide dismutase in rats.[13] Furthermore, treatment of streptozotocin-induced diabetes mellitus rats with TQ significantly reduced oxidative stress damage, inhibited the formation of malondialdehyde, increased the levels of superoxide dismutase and improved cardiovascular function.[14] Notably, it has been demonstrated that co-administration of TQ and Dox could improve the anti-tumor activity of Dox in certain cancer cell lines, such as HL-60 and multi-drug-resistant MCF-7.[15] Öztürk *et al.* and Akin *et al.* demonstrated that co-treatment with TQ and Dox could ameliorate Dox-induced hepatotoxicity and testicular toxicity in rats.[16,17] Very recently, Chen and colleagues have shown that TQ could decrease Dox-induced cardiotoxicity in mice.[18] The authors suggested that the TQ protection against Dox-induced cardiotoxicity is potentially through activation of the Nrf2/HO-1 signaling pathway and reduction of iron-mediated death, mediated primarily by Dox.[18] These results overall indicate that TQ co-treatment can reduce undesirable side effects of Dox.

In this study, we have generated a hybrid drug of TQ and Dox (Fig. 2) *via* chemical conjugation, in an attempt to generate a new compound with unique properties such as high anti-tumor activity with low normal cell toxicity, hoping to minimize the potential side effects of Dox and thereby increase its therapeutic efficacy.

2 Materials and methods

2.1 Chemicals, reagents and cell lines

Thymoquinone (TCI, Japan), doxorubicin-HCL (Biosynth Carbosynth, UK), succinic acid (Fluka, Germany) were purchased. TLC-plates SIL G-25 UV254, 20 × 20 cm (Macherey-Nagel, Germany), and silica gel, average pore size 60 Å (52–73 Å), 70–230 mesh, 63–200 μm (Sigma, USA) were used. Sulfo-NHS (*N*-hydroxysulfosuccinimide) and 1-ethyl-3-(3-dimethylaminopropyl) carbodiimide hydrochloride (EDC) were obtained from Thermo Fisher Scientific, USA. Colorimetric Cell Titer 96 non-Radioactive Cell Proliferation Assay (3-(4,5-dimethylthiazol-2-yl)-2,5-diphenyltetrazolium bromide (MTT)) (Promega, USA). ER Staining Kit-Red Fluorescence-Cytopainter (Abcam, UK). DCFDA/H2DCFDA-Cellular ROS Assay Kit (Abcam, UK). Rabbit anti-GRASP65 antibody [EPR12439]-C-terminal (Abcam, UK). Goat anti-rabbit IgG (H + L)-Alexa 647 (Thermo Fisher Scientific, USA). Human breast cancer cell line (MCF-7), glioblastoma cell line (U87), pancreatic cancer cell line (PANC-1), and lung alveolar basal epithelial cells (A549) were obtained from ATCC (USA). The primary human dermal fibroblasts (HD-fibroblasts) were isolated from a healthy 50-year-old female as previously described.[19] Human bone marrow fibroblasts (H-BM1) were obtained from Dr. Walhan Alshaer, Cell Therapy Center, Jordan.

2.2 Chemical conjugation reactions

2.2.1 Thymoquinone-succinic acid (TQ-Suc) formation. TQ was conjugated to succinic acid (Suc) (Fig. 2) by dissolving 150 mg TQ (0.93 mmol) and 87 mg succinic acid (0.75 mmol) in a 9 mL mixed solvent of acetonitrile (CH_3CN) and water (1 : 1 v/v), under an inert atmosphere (argon gas). Directly, 15 mg of silver nitrate ($AgNO_3$) (8.83×10^{-5} mmol) was added, and the mixture was left 2–3 min at RT under argon gas. The reaction mixture was heated up to 80 °C under reflux for 5 min, then 208.5 mg (0.8269 mmol) of ammonium persulfate $(NH_4)_2S_2O_8$ (dissolved in 1.5 mL distilled water) was added gradually to the reaction. The reaction mixture was refluxed at 100 °C overnight. The reaction mixture was further diluted with 0.9 mL of distilled water. Then, diethyl ether was used as an extraction solvent (5 times), and the organic layer was dried over anhydrous sodium sulfate (Na_2SO_4) powder and evaporated at atmospheric pressure overnight, providing 76.7 mg of TQ-Suc in 43% yield.

2.2.2 Thymoquinone-succinic-doxorubicin (TQ-Suc-Dox) formation. Chemical conjugation of TQ-Suc with Dox to produce the hybrid compound TQ-Suc-Dox was performed by carbodiimide chemistry. Briefly, 30.0 mg (0.1271 mmol) of TQ-Suc was dissolved in 500 μL DMSO and stirred under nitrogen gas. To activate the carboxylic acid group, 73.1 mg (0.38 mmol) of EDC was added to the TQ-Suc solution, followed by 82.8 mg (0.38 mmol) of Sulfo-NHS and stirred for 3 hours. Then, 2.5 equivalents of Dox-HCl (172.7 mg, 0.173 mmol) dissolved in 500 μL DMSO with a trace amount of TEA (22–44 μL) were added to the reaction solution, with magnetic stirring for 12–24 hours in the dark under nitrogen, providing 165 mg of the final TQ-Suc-Dox conjugate (62% yield).

2.2.3 Purification of compounds. Purification of TQ-Suc was conducted using TLC. The mobile phase used in the separation was cyclohexane/ethyl acetate/acetone (3 : 2 : 0.25). The target spot was then scratched and dissolved in methanol/ethyl acetate (1 : 1 v/v) and filtered using filter paper. For TQ-Suc-Dox purification, first, the compound was run on TLC with a mobile phase composed of ethyl acetate/dichloromethane (3 : 2) with 2% formic acid, and then the target spot was scratched and dissolved in methanol/ethyl acetate (1 : 1 v/v) and filtered using a filter paper. After evaporation of the solvent, the product was dissolved in chloroform and the supernatant was collected and purified again using silica gel column chromatography with a mobile phase of ethyl acetate/dichloromethane (3 : 1) with 2% formic acid.

2.3 Mass spectrometry analysis

High-resolution mass spectra (HR-MS) were recorded utilizing the electrospray ion trap (ESI) technique by collision-induced dissociation on a Bruker APEX-4 (7 Tesla) instrument operated under positive or negative modes to determine the molecular weights and fragmentation of the prepared conjugates. The samples were infused using a syringe pump at a flow rate of 2 μL min^{-1}.

2.4 NMR analysis

All NMR spectra were obtained using a Bruker Biospin AG Magnet system 500 MHz/54 mm instrument (Bruker BioSpin, Switzerland) with a PA BBO 500S1 BBF-H-D-05 Z SP probe, and the temperature was controlled using a variable-temperature

unit (VTU) and held constant at 298 K. Chemical shifts were measured in parts per million (ppm) and referenced to tetramethylsilane (TMS). The FID data processing and analysis were performed using Topspin 4.0.2 (Bruker Biospin GmbH, Switzerland). Deuterated solvents (99.0 atom% D; Sigma-Aldrich, USA) were used as purchased.

2.5 HPLC analysis

Purified compounds were analyzed and identified using HPLC with a UV detector (Shimadzu, Japan). The chromatographic conditions for HPLC analysis were: stationary phase of C18 universal column, isocratic elution with a mobile phase composed of methanol/acetonitrile (60 : 40 v/v), flow rate of 1 mL min^{-1}, and detection wavelength at 254 nm.

2.6 Cell cytotoxicity assay

The human cancer cell lines MCF-7, U87, PANC-1 and A549 were subjected to 3-(4,5-dimethylthiazol-2-yl)-2,5-diphenyltetrazolium bromide (MTT) cytotoxicity assay. DMSO was used as a solvent to dissolve the compounds and prepare the stock concentrations. A serial dilution of compounds was made by adding a specific volume of the stock to a calculated volume of the culture medium to obtain precise concentrations. The final percentage of DMSO was adjusted to 1% in all treatments. Briefly, the cells were seeded at a density of 5×10^3 per well in 96-well plates in appropriate medium, then treated with increasing concentrations of each compound (0.075–100 μmol L^{-1}) and incubated for 72 h at 37 °C and 5% CO_2. The Colorimetric Cell Titer 96 non-Radioactive Cell Proliferation Assay (Promega, Madison, USA) was used to detect cell proliferation in each well according to the manufacturer's instructions. The percentage viability of the cells was calculated by dividing the absorbance of the compound-treated cells by the absorbance of 1% DMSO-treated cells (control cells). Cell viability % = (absorbance of the compound-treated cells)/(absorbance of 1% DMSO control cells) × 100%.

2.7 Measurement of intracellular ROS production

Cells were seeded at a density of 20×10^3 in a black, clear-bottom 96-well plate and incubated overnight for attachment. The media were removed the next day, and 100 μL of 20 μM DCFDA diluted in media (without phenol-red) was added; the cells were incubated for 45 min in dark in an incubator at 37 °C. Then the DCFDA solution was removed and 100 μL of the compounds at different concentrations (diluted in media without phenol-red) were added and incubated for another 4 h in a 37 °C incubator in the dark. The plate was then read immediately, without washing, using a fluorescence plate reader at E_{xc}/em = 485/535 nm (GlowMax, Promega, USA). *tert*-Butyl hydrogen peroxide (TBHP) was used as a positive control in the experiment (a known generator of reactive oxygen species (ROS)).

2.8 Subcellular localization and confocal laser scanning microscopy

MCF-7 cells were seeded into 24-well culture plates containing glass coverslips and incubated with their compatible culture medium for 24 h in a tissue culture incubator (37 °C, 95% humidity and 5% CO_2). After incubation, the culture medium was removed and the cells were treated with 100 μM of either Dox or TQ-Suc-Dox (diluted in complete culture medium). Then, the uptake of drugs was performed at 37 °C for the indicated time points. The cells were then washed twice with PBS and fixed in 4% formaldehyde for 15 min at room temperature in the dark. The fixed cells were then quenched in 50 mM ammonium chloride (NH_4Cl) for 5 min to decrease possible auto-fluorescence. DAPI was used to stain the nucleus of the cells. The confocal images were acquired using an LSM 780 (Zeiss, Germany). The objective lens used for acquiring the images was a Plan-Apochromat 63X/1.4 NA Oil DIC M27. Laser wavelengths of 405 nm, 488 nm, 561 nm and 633 nm were used for excitation of the nuclear stain DAPI, Dox, ER red-cytopainter, and Alexa-Fluor 647, respectively. The detection range for fluorescence emission signals was: 420–520 nm for DAPI, 535–599 nm for Dox, 600–712 nm for ER red-cytopainter, and 637–755 nm for Alexa-Fluor 647.

2.9 Fluorescence and co-localization quantitation

Quantitation of nuclear and cytoplasmic localization of TQ-Suc-Dox and free Dox compounds was conducted by measuring the fluorescence intensity within the region of interest using Image J software. The degree of co-localization between the TQ-Suc-Dox and organelle markers (Golgi and ER) was determined by calculating Manders' and Pearson's coefficients. The colocalization parameters were the Pearson's correlation coefficient, which measures linear correlation between the two channels, and the Manders coefficient, which calculates the percentage of the total signal from one channel that overlaps with the signal from another, were measured using the plugin JACoP on Image J software.

2.10 Fluorescence live-cell imaging

For live-cell imaging, cells were grown as monolayers on a 4.55 cm^2 cell culture slide (SPL Life Sciences, Korea). All live-cell imaging experiments were performed with a Zeiss AxioObserver Z1 Fluorescence Microscope. Live cells were imaged at 37 °C and 5% CO_2. For ER staining, the dye was diluted 1/500 in 1× assay buffer and incubated with cells for 15 min at 37 °C. The cells were washed twice with 1× PBS and pulsed with either TQ-Suc-Dox or free Dox compounds for 5 min at 37 °C, and washed three times with PBS. Then, 1 mL of PBS was added and cells were imaged live for 45 min at 37 °C. Dox was excited using a 470 nm solid-state laser diode. ER red-cytopainter was excited using a 555 nm solid-state laser diode. Fluorescence signals were collected using the following bandwidths: 490–570 nm for Dox and 577–617 nm for ER red-cytopainter. Image acquisition was performed using an LD A-Plan 40x/0.55 Objective.

2.11 Statistical analysis

Statistical analysis was performed using GraphPad Prism 9.4.0. The *t*-test was used to measure the significance of the data. *P*-values < 0.05 were considered statistically significant, ***P < 0.001. **P < 0.01. *P < 0.05.

3 Results and discussion

3.1 Preparation and characterization of the TQ-Suc-Dox hybrid compound

The formation of the TQ-Suc-Dox conjugate was confirmed using ^{1}H, ^{13}C-dept135, ^{1}H–^{13}C-HMQC, and ^{1}H–^{15}N-HMBC NMR experiments (SI Fig. S1 and S2). ^{1}H NMR (500 MHz, DMSO-d_6) for TQ-Suc-Dox conjugates; $\delta = 1.1$ (s, 6H, $(CH_3)_2$), 1.5 (s, 3H, b), 1.9 (s, 3H, CH_3–TQ), 2.1 (s, 2H, H-4), 2.9 (s, 2H, CH–TQ), 3.5 (m, 4H, CH_2–Suc, c), 3.7 (m, 1H, d), 3.95 (s, 3H, OCH_3), 4.1 (m, 1H, e), 4.56 (m, 1H, H-1), 4.9 (s, 1H, 1-OH), 4.9 (m, 1H, H-5), 5.2 (m, 1H, a), 5.3 (s, 1H, 3-OH), 7.6 (d, 1H, H-19), 7.7 (d, 1H, H-20), 7.9 (d, 1H, H-18), ~14 (br s, 2H, 9-OH and 10-OH). In addition, the amine group (–NH_2) in doxorubicin, which typically appears at ~7.8 ppm (^{1}H) and ~42.6 ppm (^{15}N), was converted into an amide group (–CO–NH–), observed at 7.5 ppm (^{1}H) and 150.2 ppm (^{15}N), as shown in SI Fig. S2, consistent with literature-reported values. MS (ESI) (positive mode) *m/z* calculated for $C_{40}H_{43}NO_{14}$ $[M + Na^+]^+$: 784.25758, found: 784.25892 (SI Fig. S3). MS (ESI) (negative mode) *m/z* calculated for $C_{40}H_{43}NO_{14}$ $[M - H^+]^-$: 760.26108, found 760.26023 (SI Fig. S3). For purity detection of the generated TQ-Suc-Dox compound, the compound was analyzed using HPLC (Shimadzu, Japan), and ~90% purity was determined for the compound (SI Fig. S4).

3.2 The cytotoxic effect of the TQ-Suc-Dox hybrid on the growth of cancer and normal cells

The TQ-Suc-Dox compound was tested against different types of cancer cell lines, including MCF-7, U87, PANC-1 and A549. The results were then compared to those obtained with the free drugs TQ and Dox. Interestingly, TQ-Suc-Dox showed high antitumor activity against all tested cell lines (average IC_{50} ~10 μM) (Fig. 3). On comparison, free Dox showed very high cytotoxicity against all the cell lines (average IC_{50} ~0.4 μM) (Fig. 3), whereas TQ showed the least effect on the cell lines, with an average IC_{50} of ~32 μM (Fig. 3). Strikingly, TQ-Suc-Dox exerted the highest cytotoxicity (IC_{50} ~2 μM) on MCF-7 breast cancer cells, indicating a possible selectivity in the action of the hybrid compound against breast cancer cells. Notably, the cytotoxic activity results for free Dox and TQ against MCF-7 cancer cells showed IC_{50} values of ~0.3 μM and 23 μM, respectively, which are consistent with the literature.[15] It is worth mentioning that MCF-7 cells are a well-characterized human breast cancer cell line that are frequently used in research due to their expression

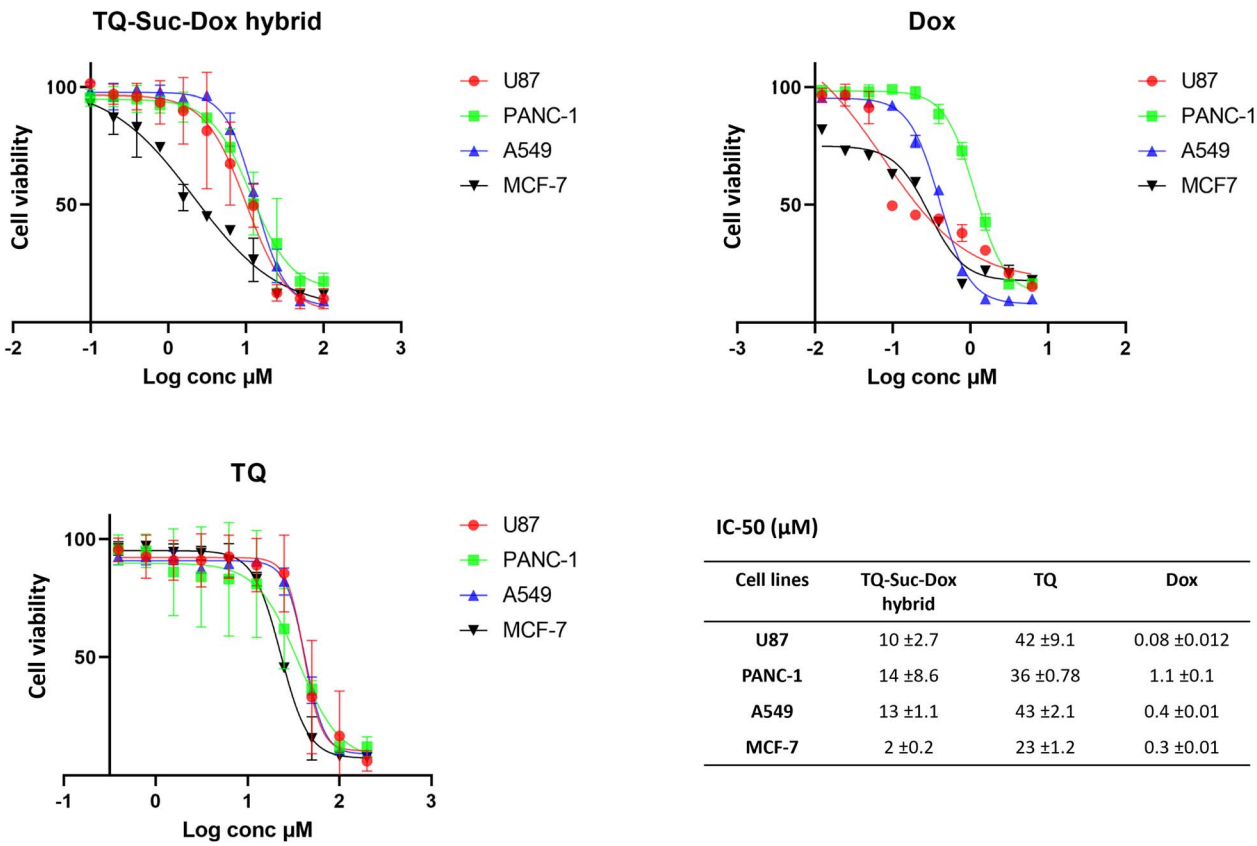

IC-50 (μM)

Cell lines	TQ-Suc-Dox hybrid	TQ	Dox
U87	10 ±2.7	42 ±9.1	0.08 ±0.012
PANC-1	14 ±8.6	36 ±0.78	1.1 ±0.1
A549	13 ±1.1	43 ±2.1	0.4 ±0.01
MCF-7	2 ±0.2	23 ±1.2	0.3 ±0.01

Fig. 3 Cell cytotoxicity and determination of IC_{50} values of TQ-Suc-Dox hybrid, TQ and Dox compounds in cancer cells. The survival percentages of cancer cell lines (MCF-7, U87, PANC-1 and A549) after treatment with different log concentrations of TQ-Suc-Dox, TQ and Dox and incubation for 72 h at 37 °C and 5% CO_2 were determined. DMSO was used as a solvent to dissolve compounds and prepare stock concentrations. A serial dilution of compounds was made by adding a specific volume of the stock to a calculated volume of the culture medium to obtain precise concentrations. The final percentage of DMSO was adjusted to 1% in all treatments. The colorimetric MTT cytotoxicity assay was used to detect cell survival. Data expressed as mean ± SD. IC_{50}: half-maximal inhibitory concentration.

of estrogen receptor (ER) and progesterone receptor (PR), making them a relevant model to study ER+ and PR+ breast cancer cells.[20] The selective, high efficacy of the compound against MCF-7 cells is very interesting, and could be due to drug targeting of a specific signaling pathway mainly involved in breast cancer tumorigenesis. Indeed, several signaling pathways and molecular networks have been demonstrated to play a critical role in controlling important pro-survival and pro-growth cellular processes in breast cancers, including mitogen-activated protein (MAP) kinase, PI3K/Akt/nuclear factor kappa B (NF-κB), TGF-β, hedgehog (Hh), Notch, Wnt/β-catenin, and Hippo pathways.[21] However, the detailed molecular mechanism by which the compound kills MCF-7 cancer cells needs to be investigated in the future.

On the other hand, the TQ-Suc-Dox showed relatively minimal cytotoxicity on normal cells, including human-derived bone marrow fibroblasts (H-BM1) and dermal fibroblasts (HD-fibroblasts) (IC_{50} ~16 μM and ~10 μM, respectively), compared to the free Dox, which showed very high toxicity on these cells (IC_{50} ~0.2 μM, ~0.1 μM, respectively) (Fig. 4). Overall, these results clearly demonstrate that the generated TQ-Suc-Dox compound is capable of killing tumor cells, particularly invasive ER+ and PR+ breast adenocarcinoma, with high efficiency while exerting low toxicity on normal cells.

3.3 The TQ-Suc-Dox hybrid generates less ROS in cells compared to free Dox

The intracellular levels of reactive oxidative species (ROS), including hydroxyl (˙OH) and peroxyl (ROO˙) radicals, which are important mediators of Dox-induced side toxicity, were measured in live cell samples by a fluorometric assay. Our results demonstrate a significant increase in ROS levels in both MCF-7 and human dermal fibroblast cells treated with either free Dox or TQ-Suc-Dox, compared to the intracellular ROS levels measured in cells treated with DMSO (Fig. 5). As expected, free Dox demonstrated a dose-dependent increase in ROS production in the two cell lines (Fig. 5A and B). Interestingly, ROS production in cells treated with 10 μM of TQ-Suc-Dox was significantly lower than that produced by the free Dox (Fig. 5A and B).

The decrease in ROS production in cells treated with TQ-Suc-Dox compared to free Dox could be related to the presence of TQ. Indeed, TQ is well known to act as a scavenger of free radicals,[22,23] and it could potentially decrease the side toxicity associated with Dox-generated ROS. In fact, co-treating cells with free TQ has been shown to reduce the side toxicity of drugs such as aflatoxin B, Dox and cisplatin.[12,17,24] It has been hypothesized in previous studies that Dox may induce cardiotoxicity of the myocardium *via* Dox-induced oxidative

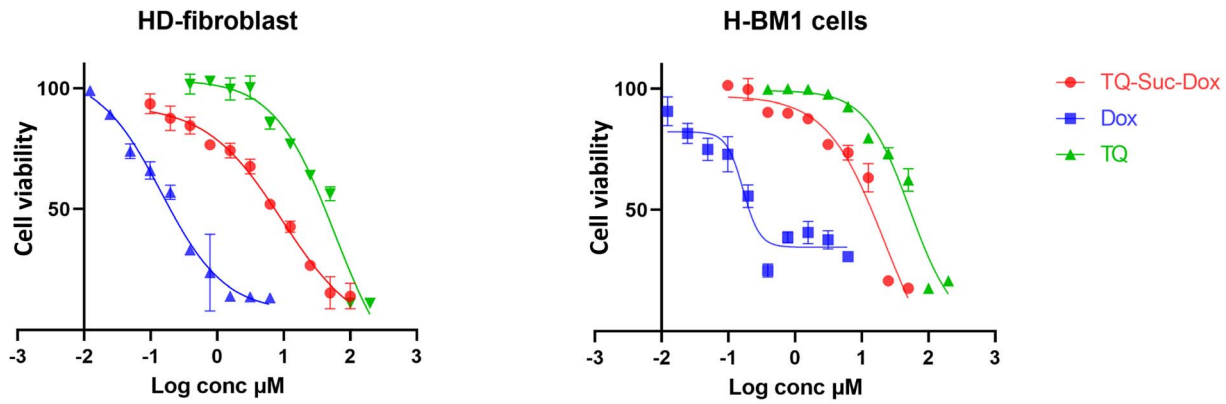

IC-50 (μM)

Cell lines	TQ-Suc-Dox hybrid	TQ	Dox
HD-fibroblast	10 ± 2.2	58 ± 2.4	0.134 ± 0.07
H-BM1	16 ± 1.4	53 ± 8.7	0.161 ± 0.03

Fig. 4 Cell cytotoxicity of TQ-Suc-Dox hybrid, TQ and Dox compounds in normal human cells. MTT cytotoxicity assays show the survival percentage of human fibroblast cells (HD-fibroblast) and human bone marrow fibroblasts (H-BM1) after treatment with different log concentrations of TQ-Suc-Dox, TQ and Dox, incubated for 72 h at 37 °C and 5% CO_2. DMSO was used as a solvent to dissolve compounds and prepare stock concentrations. A serial dilution of compounds was performed by adding a specific volume of the stock to a calculated volume of the culture medium to obtain precise concentrations. The final percentage of DMSO was adjusted to 1% in all treatments. Data expressed as mean ± SD. IC_{50}: half-maximal inhibitory concentration.

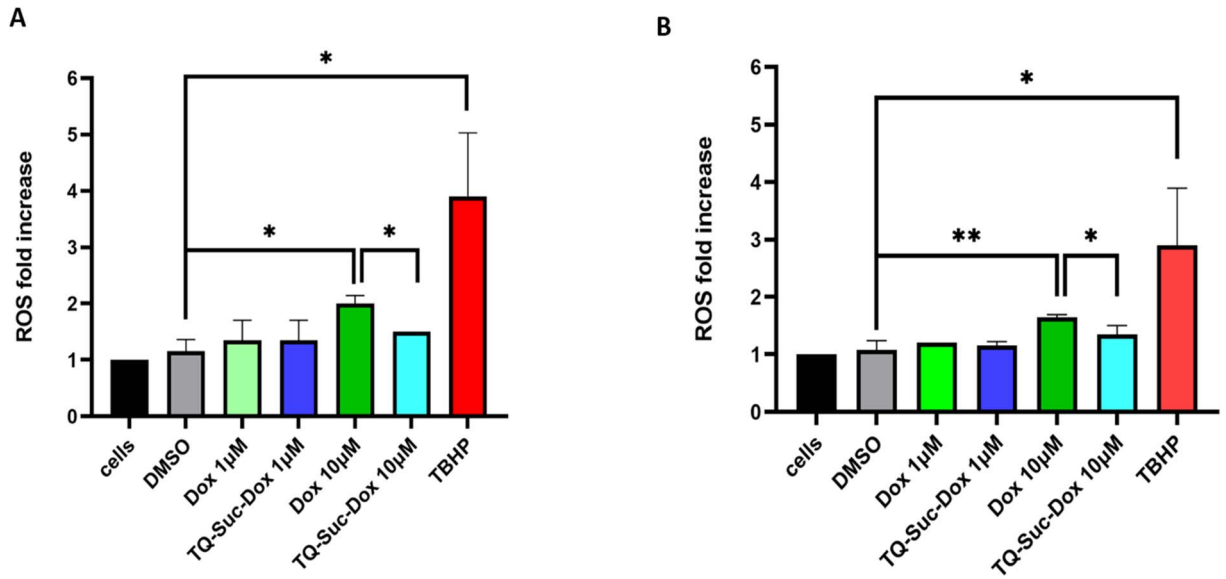

Fig. 5 Measurement of intracellular ROS production in cells after treatment with TQ, free Dox and TQ-Suc-Dox compounds. DCFDA/H2DCFDA-cellular ROS assays were conducted to measure intracellular ROS production in cells: (A) MCF-7 and (B) HD-fibroblasts. The cells were seeded in black, clear-bottom 96-well plates. DCFDA diluted in media was added and incubated for 45 min in a 37 °C incubator in dark. Then, DCFDA solution was removed and compounds at different concentrations were added and incubated for another 4 h in a 37 °C incubator in dark. DMSO was used as a solvent to dissolve compounds in ROS assays. The plate was then read immediately using a fluorescence plate reader at E_{xc}/em = 485/535 nm. *P*-values were calculated using the unpaired, one-tailed *t*-test. *$p < 0.05$. **$p < 0.01$. TBHP (*tert*-butyl hydrogen peroxide) was used as a positive control in the experiment.

stress.[25,26] Interestingly, co-treatment of mice with Dox and TQ was shown to increase the level of antioxidant proteins, including GSH, catalase and superoxide dismutase, reduce lipid peroxidation, and protect against Dox-induced cardiotoxicity.[27] Furthermore, Miyoshi *et al.* recently demonstrated that Dox-induced cardiotoxicity in rats can be ameliorated *in vivo via* co-treatment with the antioxidant LCZ696 (sacubitril/valsartan).[26]

3.4 Subcellular localization of the TQ-Suc-Dox hybrid in breast cancer cells is mainly to the endoplasmic reticulum

To determine the internalization and subcellular localization of the TQ-Suc-Dox hybrid compound in comparison to free Dox, an internalization assay was employed, followed by confocal laser scanning microscopy (CLSM) analysis. Breast cancer cell line (MCF-7) was treated with either TQ-Suc-Dox or free Dox and incubated at 37 °C for over 4 h for continuous uptake experiments. Both TQ-Suc-Dox and free doxorubicin were efficiently internalized; after uptake for 1 h, almost all the Dox was localized in the nucleus (Fig. 6A), and only a minor amount could be detected in the cytoplasm of cells. The same results were demonstrated at 4 h uptake. Strikingly, most TQ-Suc-Dox molecules, for both 1 h and 4 h uptake experiments, were found to be located in the perinuclear-like regions in the cytoplasm of the cells (Fig. 6C). To further define these regions, we co-stained these structures with either *cis*-Golgi GRASP65 marker or ER stain (Fig. 7). Our results show, for both 1 h and 4 h uptake experiments, high co-localization between TQ-Suc-Dox and ER organelles (90%) (Fig. 7B), compared to very little co-localization between TQ-Suc-Dox and Golgi apparatus (≤20%) (Fig. 7A). Indicating that the hybrid compound is mainly localized to the ER region. Furthermore, we analyzed the real-time uptake of TQ-Suc-Dox and free Dox and their distribution in live MCF-7 cells using the fluorescence live-cell imaging technique (Fig. 8). For the TQ-Suc-Dox, we observed intense intracellular fluorescence after 5 min uptake (pulse-period), and the compound was then predominantly accumulated in the ER over the 45 min chase-period (Fig. 8A). For the free Dox, the drug showed intense intracellular fluorescence after the 10 min pulse-period, and then it was predominantly localized in the nucleus over the chase-period (Fig. 8B).

In fact, the spatial localization of drugs within the cell is an important factor that has been proposed to play a major role in improving efficacy and minimizing toxicity of drugs.[28] Notably, changing the subcellular localization of Dox has been reported previously. Indeed, Buondonno *et al.* have demonstrated that bio-conjugation of Dox with a H_2S donor substructure, to produce a H_2S-releasing Dox (Sdox) compound, resulted in the accumulation of the compound within the ER[29] and caused less hepatotoxicity and oxidative damage compared to free Dox.[30] Also, targeting Dox to the ER could be of great significance for decreasing the potential side-toxicity of Dox provoked by the nuclear-localization of Dox and subsequent DNA damage,[31] as well as for overcoming Dox-resistance in cancer cells.[29,30]

It is worth mentioning that the ER is a large network of folded membrane-enclosed tubules and sacs that extend from the nuclear membrane throughout the cytoplasm. Its functions in cells include calcium storage, protein synthesis and lipid metabolism.[32] Therefore, under ER stress, unfolded or

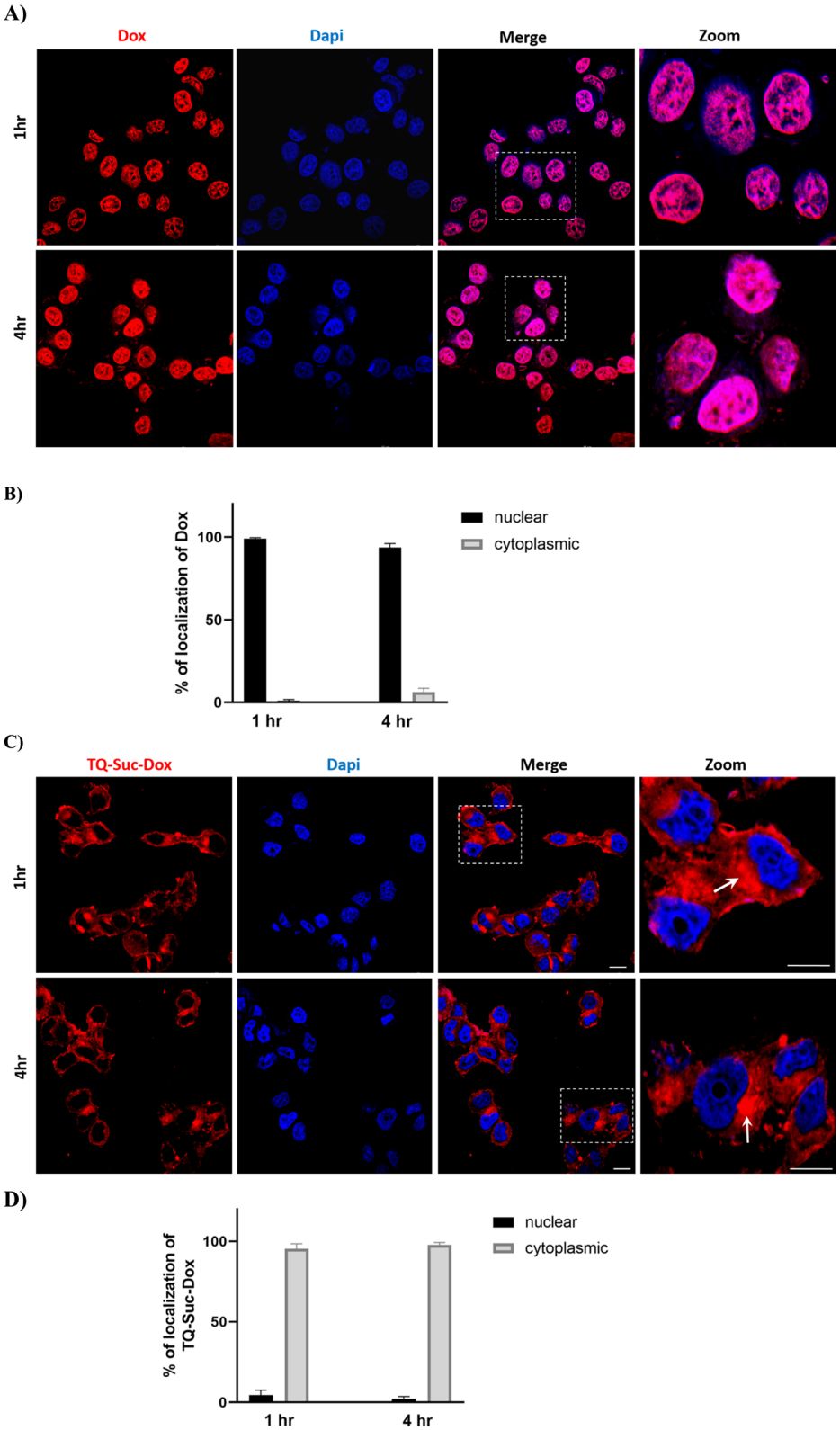

Fig. 6 Cellular uptake and localization of Dox and TQ-Suc-Dox compounds Confocal laser scanning microscopy (CLSM) analyses for the uptake of (A) free Dox or (C) TQ-Suc-Dox in cultured MCF-7 cells. For internalization, MCF7 cells were incubated with free Dox or TQ-Suc-Dox compounds for 1 h and 4 h time points. All cells were fixed in 4% paraformaldehyde and nuclei stained with DAPI (blue color). Doxorubicin and TQ-Suc-Dox compounds are shown in red color. White arrows indicate accumulation of the TQ-Suc-Dox in perinuclear-like regions. Scale bars represent 10 μm. Quantitation of nuclear and cytoplasmic localization of free Dox (B) and TQ-Suc-Dox (D) was conducted by measuring the fluorescence intensity within the region of interest using the Image J software. Data are expressed as the mean ± SD (10 cells for each time point).

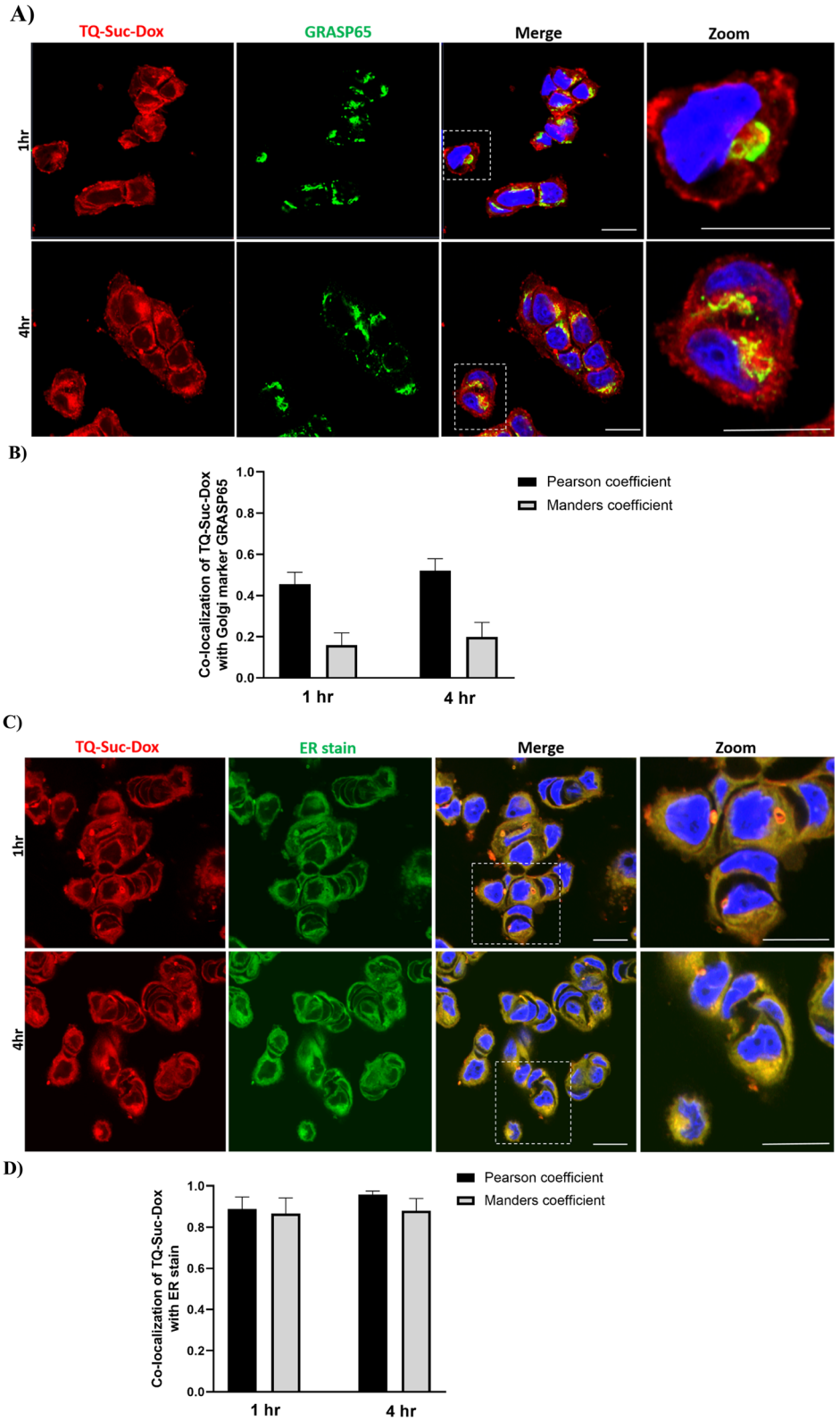

Fig. 7 Cellular uptake and subcellular localization of the TQ-Suc-Dox in Golgi/ER organelles. Confocal laser scanning microscopy (CLSM) analyses for the uptake of TQ-Suc-Dox compound in cultured MCF-7 cells. For colocalization with (A) Golgi marker (GRASP65) and (C) ER marker. MCF7 cells were incubated with TQ-Suc-Dox compound for 1 h and 4 h time points. All cells were fixed in 4% paraformaldehyde and nuclei stained with DAPI (blue color). TQ-Suc-Dox compounds are shown in red. Golgi and ER markers are shown in green. Scale bars represent 10 μm. Quantitation of co-localization between TQ-Suc-Dox and organelle markers for Golgi (B) and ER (D) was determined by calculating Manders' and Pearson's coefficients using the plugin JACoP on Image J software. Data is expressed as the mean ± SD (10 cells for each time point).

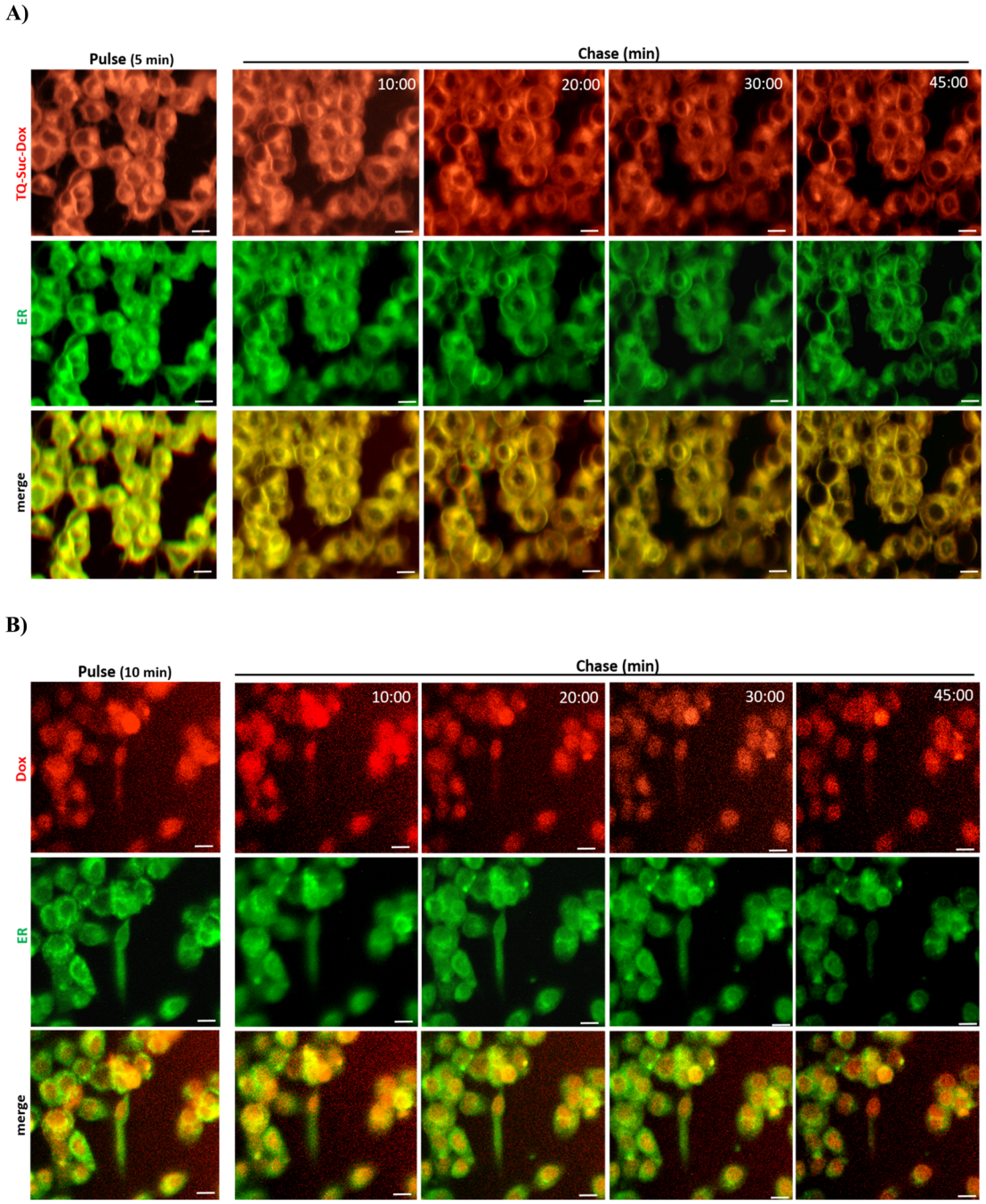

Fig. 8 Live-cell imaging analysis of the dynamic trafficking of the TQ-Suc-Dox compared to the free Dox in MCF-7 cells. Fluorescence live-cell imaging analyses for the uptake of (A) TQ-Suc-Dox and (B) free Dox in cultured MCF-7 cells. Cells were exposed to the compounds in the form of a short pulse (5 or 10 min), washed three times with PBS, and then chased by acquiring 2D images every 30 s for 45 min at 37 °C. TQ-Suc-Dox and Dox compounds are shown in red. ER stain is shown in green. Scale bars represent 10 μm.

misfolded proteins could accumulate in the ER lumen and disrupt ER homeostasis, which may eventually initiate a cascade of reactions to activate programmed cell death pathways.[33] Thus, it is reasonable to think that ER targeting might enhance the efficacy of chemotherapeutic drugs and provide new anticancer targets. Indeed, strategies for targeting the ER have been previously proposed to develop new effective anticancer agents.[33–35] For example, it has been shown that thapsigargin compounds induce apoptosis in cancer cells by binding and disrupting the ER-Ca^{2+} pump, causing ER Ca^{2+} depletion and subsequent ER stress, which eventually activates the apoptosis enzymes caspase-8 and caspase-3.[36]

Finally, in our case, both the presence of TQ (antioxidant) and the spatial sub-cellular localization of the TQ-Suc-Dox to the ER could contribute to the low side-toxicity of the compound that was observed in normal cells.

4 Conclusion

Dox is one of the most effective chemotherapies in clinical practice; however, factors including acute and chronic side effects and the rapid development of resistance have limited its use. On the other hand, TQ has shown chemopreventive characteristics when combined with other chemotherapeutics. In this study, the conjugate TQ-Suc-Dox has been demonstrated to exert efficient antitumor activity against different types of cancer cells; in particular, adenocarcinoma breast cancer cells MCF-7. In contrast, low toxicity of the drug was detected in normal cells such as human bone marrow and dermal fibroblast.

On the other side, the subcellular accumulation of TQ-Suc-Dox in the ER indicates that the drug may directly affect this organelle, which has a central role in lipid and protein biosynthesis. Notably, induction of ER stress was reported as a key contributor to Dox-induced cardiotoxicity.[37,38] However, TQ has been demonstrated to protect the rat liver against ischemia–reperfusion (I/R) injury by preventing ER stress and mitochondrial dysfunction.[39] Also, researchers have recently reported the role of TQ in reducing the ER stress caused by Dox in animal models.[40,41] Nevertheless, further research in the future is needed to explain mechanistically how TQ-Suc-Dox could affect the function of the ER in cells.

To conclude, we think that the generated TQ-Suc-Dox could be beneficial for therapeutic purposes under various scenarios. Firstly, the side-toxicity related to the therapeutic compound may be significantly reduced because of its antioxidant properties and low toxicity in normal cells. Secondly, and importantly, the specific intracellular targeting of the drug to the ER will overcome one of the most critical limitations of Dox application, drug resistance, which has been a major hurdle in Dox-resistant cancer chemotherapy.[42,43] However, future experiments will be necessary to evaluate the cytotoxicity of the compound *in vivo* as well as in various Dox-resistant models. Additionally, the mechanism by which the compound kills cancer cells and its potential selectivity against adenocarcinoma breast cancer cells need to be investigated.

Patent

The generated compound described in this study has been registered for a patent in the World Intellectual Property Organization (WIPO). Title: a pharmaceutical compound, method of preparation thereof, and its use for treating cancer. Publication number: WO/2025/158476. International application number: PCT/JO2025/050001. International filing date: 21.01.2025. Publication date: 31.07.2025.

Conflicts of interest

There are no conflicts of interest to declare.

Data availability

All underlying data are available within the article and its supplementary information (SI) file. Supplementary information is available. See DOI: **https://doi.org/10.1039/d5ra05492c**.

Acknowledgements

This work was supported by funding from the Scientific Research and Innovation Support Fund, Ministry of Higher Education and Scientific Research, Jordan (Grant number: MPH/2/24/2017). We would like to thank Dr Nidaa Ababneh, Cell Therapy Centre, The University of Jordan, for providing the human dermal fibroblasts.

References

1 D. Hanahan and R. A. Weinberg, Hallmarks of cancer: the next generation, *Cell*, 2011, **144**(5), 646–674, DOI: **10.1016/j.cell.2011.02.013**.
2 J. Sun, Q. Wei, Y. Zhou, J. Wang, Q. Liu and H. Xu, A systematic analysis of FDA-approved anticancer drugs, *BMC Syst. Biol.*, 2017, **11**(5), 87, DOI: **10.1186/s12918-017-0464-7**.
3 O. Tacar, P. Sriamornsak and C. R. Dass, Doxorubicin: an update on anticancer molecular action, toxicity and novel drug delivery systems, *J. Pharm. Pharmacol.*, 2013, **65**(2), 157–170, DOI: **10.1111/j.2042-7158.2012.01567.x**.
4 I. Alfreahat, H. Nsairat, I. D. Aldeeb, A. Al-Samydai and W. Alshaer, *In Vitro* Potentiation of Doxorubicin Cytotoxicity Utilizing Clarithromycin Loaded-PEGylated Liposomes, *Technol. Cancer Res. Treat.*, 2025, **24**, 15330338241312561, DOI: **10.1177/15330338241312561**.
5 E. Abu Saleem, Z. Lafi, N. Shalan, W. Alshaer and I. Hamadneh, Formation and evaluation of doxorubicin and cromoglycate metal-organic framework for anti-cancer activity, *Nanomedicine*, 2025, **20**(5), 467–479, DOI: **10.1080/17435889.2025.2459059**.
6 S. Y. Kim, S. J. Kim, B. J. Kim, S. Y. Rah, S. M. Chung, M. J. Im and U. H. Kim, Doxorubicin-induced reactive oxygen species generation and intracellular Ca2+ increase are reciprocally modulated in rat cardiomyocytes, *Exp. Mol. Med.*, 2006, **38**(5), 535–545, DOI: **10.1038/emm.2006.63**.
7 P. S. Rawat, A. Jaiswal, A. Khurana, J. S. Bhatti and U. Navik, Doxorubicin-induced cardiotoxicity: An update on the molecular mechanism and novel therapeutic strategies for effective management, *Biomed. Pharmacother.*, 2021, **139**, 111708, DOI: **10.1016/j.biopha.2021.111708**.
8 C. Carvalho, R. X. Santos, S. Cardoso, S. Correia, P. J. Oliveira, M. S. Santos and P. I. Moreira, Doxorubicin: the good, the bad and the ugly effect, *Curr. Med. Chem.*, 2009, **16**(25), 3267–3285, DOI: **10.2174/092986709788803312**.
9 S. Darakhshan, A. Bidmeshki Pour, A. Hosseinzadeh Colagar and S. Sisakhtnezhad, Thymoquinone and its therapeutic potentials, *Pharmacol. Res.*, 2015, **95–96**, 138–158, DOI: **10.1016/j.phrs.2015.03.011**.
10 C. Sarkar, S. Jamaddar, T. Islam, M. Mondal, M. T. Islam and M. S. Mubarak, Therapeutic perspectives of the black cumin component thymoquinone: A review, *Food Funct.*, 2021, **12**(14), 6167–6213, DOI: **10.1039/d1fo00401h**.
11 G. Tiwari, M. Gupta, L. D. Devhare and R. Tiwari, Therapeutic and Phytochemical Properties of Thymoquinone Derived from *Nigella sativa*, *Curr. Drug Res.*

Rev., 2024, **16**(2), 145–156, DOI: 10.2174/2589977515666230811092410.

12 A. Nili-Ahmadabadi, F. Tavakoli, G. Hasanzadeh, H. Rahimi and O. Sabzevari, Protective effect of pretreatment with thymoquinone against Aflatoxin B(1) induced liver toxicity in mice, *Daru*, 2011, **19**(4), 282–287.

13 M. A. Randhawa, M. S. Alghamdi and S. K. Maulik, The effect of thymoquinone, an active component of Nigella sativa, on isoproterenol induced myocardial injury, *Pak. J. Pharm. Sci.*, 2013, **26**(6), 1215–1219.

14 H. Liu, H. Y. Liu, Y. N. Jiang and N. Li, Protective effect of thymoquinone improves cardiovascular function, and attenuates oxidative stress, inflammation and apoptosis by mediating the PI3K/Akt pathway in diabetic rats, *Mol. Med. Rep.*, 2016, **13**(3), 2836–2842, DOI: 10.3892/mmr.2016.4823.

15 K. Effenberger-Neidnicht and R. Schobert, Combinatorial effects of thymoquinone on the anti-cancer activity of doxorubicin, *Cancer Chemother. Pharmacol.*, 2011, **67**(4), 867–874, DOI: 10.1007/s00280-010-1386-x.

16 E. Öztürk, E. Kaymak, A. T. Akin, D. Karabulut, H. M. Ünsal and B. Yakan, Thymoquinone is a protective agent that reduces the negative effects of doxorubicin in rat testis, *Hum. Exp. Toxicol.*, 2020, **39**(10), 1364–1373, DOI: 10.1177/0960327120924108.

17 A. T. Akin, E. Öztürk, E. Kaymak, D. Karabulut and B. Yakan, Therapeutic effects of thymoquinone in doxorubicin-induced hepatotoxicity *via* oxidative stress, inflammation and apoptosis, *Anat. Histol. Embryol.*, 2021, **50**(6), 908–917, DOI: 10.1111/ahe.12735.

18 Y. Chen, W. Luo and Y. Wu, Protective effect of thymoquinone against doxorubicin-induced cardiotoxicity and the underlying mechanism, *Toxicol. Appl. Pharmacol.*, 2024, **5**, 117179, DOI: 10.1016/j.taap.2024.117179.

19 N. A. Ababneh, B. Al-Kurdi, D. Ali, R. Barham, N. Sharar, M. M. Mrahleh, B. Salah and A. Awidi, Generation of a human induced pluripotent stem cell (iPSC) line (JUCTCi011-A) from skin fibroblasts of a healthy Jordanian male subject, *Stem Cell Res.*, 2020, **48**, 101923, DOI: 10.1016/j.scr.2020.101923.

20 Ș. Comșa, A. M. Cîmpean and M. Raica, The Story of MCF-7 Breast Cancer Cell Line: 40 years of Experience in Research, *Anticancer Res.*, 2015, **35**(6), 3147–3154.

21 S. Yousefnia, F. Seyed Forootan, S. Seyed Forootan, M. H. Nasr Esfahani, A. O. Gure and K. Ghaedi, Mechanistic Pathways of Malignancy in Breast Cancer Stem Cells, *Front. Oncol.*, 2020, **10**, 452, DOI: 10.3389/fonc.2020.00452.

22 O. A. Badary, R. A. Taha, A. M. Gamal el-Din and M. H. Abdel-Wahab, Thymoquinone is a potent superoxide anion scavenger, *Drug Chem. Toxicol.*, 2003, **26**(2), 87–98, DOI: 10.1081/dct-120020404.

23 C. C. Woo, A. P. Kumar, G. Sethi and K. H. Tan, Thymoquinone: potential cure for inflammatory disorders and cancer, *Biochem. Pharmacol.*, 2012, **83**(4), 443–451, DOI: 10.1016/j.bcp.2011.09.029.

24 M. Al Fayi, H. Otifi, M. Alshyarba, A. A. Dera and P. Rajagopalan, Thymoquinone and curcumin combination protects cisplatin-induced kidney injury, nephrotoxicity by attenuating NFκB, KIM-1 and ameliorating Nrf2/HO-1 signalling, *J. Drug Target.*, 2020, **28**(9), 913–922, DOI: 10.1080/1061186X.2020.1722136.

25 M. F. Xu, P. L. Tang, Z. M. Qian and M. Ashraf, Effects by doxorubicin on the myocardium are mediated by oxygen free radicals, *Life Sci.*, 2001, **68**(8), 889–901, DOI: 10.1016/s0024-3205(00)00990-5.

26 T. Miyoshi, K. Nakamura, N. Amioka, O. F. Hatipoglu, T. Yonezawa, Y. Saito, M. Yoshida, S. Akagi and H. Ito, LCZ696 ameliorates doxorubicin-induced cardiomyocyte toxicity in rats, *Sci. Rep.*, 2022, **12**(1), 4930, DOI: 10.1038/s41598-022-09094-z.

27 M. F. Alam, G. Khan, M. M. Safhi, S. Alshahrani, R. Siddiqui, S. Sivagurunathan Moni and T. Anwer, Thymoquinone Ameliorates Doxorubicin-Induced Cardiotoxicity in Swiss Albino Mice by Modulating Oxidative Damage and Cellular Inflammation, *Cardiol. Res. Pract.*, 2018, **2018**, 1483041, DOI: 10.1155/2018/1483041.

28 N. M. Sakhrani and H. Padh, Organelle targeting: third level of drug targeting, *Drug Des. Dev. Ther.*, 2013, **7**, 585–599, DOI: 10.2147/DDDT.S45614.

29 I. Buondonno, E. Gazzano, E. Tavanti, K. Chegaev, J. Kopecka, M. Fanelli, B. Rolando, R. Fruttero, A. Gasco, C. Hattinger, M. Serra and C. Riganti, Endoplasmic reticulum-targeting doxorubicin: a new tool effective against doxorubicin-resistant osteosarcoma, *Cell. Mol. Life Sci.*, 2019, **76**(3), 609–625, DOI: 10.1007/s00018-018-2967-9.

30 P. Alov, M. Al Sharif, D. Aluani, K. Chegaev, J. Dinic, A. Divac Rankov, M. X. Fernandes, F. Fusi, A. T. García-Sosa, R. Juvonen, M. Kondeva-Burdina, J. M. Padrón, I. Pajeva, T. Pencheva, A. Puerta, H. Raunio, C. Riganti, I. Tsakovska, V. Tzankova, Y. Yordanov and S. Saponara, A Comprehensive Evaluation of Sdox, a Promising H_2S-Releasing Doxorubicin for the Treatment of Chemoresistant Tumors, *Front. Pharmacol*, 2022, **13**, 831791, DOI: 10.3389/fphar.2022.831791.

31 K. M. Tewey, T. C. Rowe, L. Yang, B. D. Halligan and L. F. Liu, Adriamycin-induced DNA damage mediated by mammalian DNA topoisomerase II, *Science*, 1984, **226**(4673), 466–468, DOI: 10.1126/science.6093249.

32 D. S. Schwarz and M. D. Blower, The endoplasmic reticulum: structure, function and response to cellular signaling, *Cell. Mol. Life Sci.*, 2016, **73**(1), 79–94, DOI: 10.1007/s00018-015-2052-6.

33 J. Boelens, S. Lust, F. Offner, M. E. Bracke and B. W. Vanhoecke, Review. The endoplasmic reticulum: a target for new anticancer drugs, *In Vivo*, 2007, **21**(2), 215–226.

34 D. Wlodkowic, J. Skommer, D. McGuinness, C. Hillier and Z. Darzynkiewicz, ER-Golgi network–a future target for anti-cancer therapy, *Leuk. Res.*, 2009, **33**(11), 1440–1447, DOI: 10.1016/j.leukres.2009.05.025.

35 L. Xu, F. Peng, Q. Luo, Y. Ding, F. Yuan, L. Zheng, W. He, S. S. Zhang, X. Fu, J. Liu, *et al.*, IRE1α silences dsRNA to prevent taxane-induced pyroptosis in triple-negative breast

cancer, *Cell*, 2024, **187**(25), 7248–7266, DOI: 10.1016/j.cell.2024.09.032.

36 P. Lindner, S. B. Christensen, P. Nissen, J. V. Møller and N. Engedal, Cell death induced by the ER stressor thapsigargin involves death receptor 5, a non-autophagic function of MAP1LC3B, and distinct contributions from unfolded protein response components, *Cell Commun. Signal.*, 2020, **18**(1), 12, DOI: 10.1186/s12964-019-0499-z.

37 F. Yarmohammadi, R. Rezaee, A. W. Haye and G. Karimi, Endoplasmic reticulum stress in doxorubicin-induced cardiotoxicity may be therapeutically targeted by natural and chemical compounds: A review, *Pharmacol. Res.*, 2021, **164**, 105383, DOI: 10.1016/j.phrs.2020.105383.

38 M. Sun, X. Zhang, B. Tan, Q. Zhang, X. Zhao and D. Dong, Potential role of endoplasmic reticulum stress in doxorubicin-induced cardiotoxicity-an update, *Front. Pharmacol.*, 2024, **15**, 1415108, DOI: 10.3389/fphar.2024.1415108.

39 A. Bouhlel, I. Ben Mosbah, N. Hadj Abdallah, C. Ribault, R. Viel, S. Mannaï, A. Corlu and H. Ben Abdennebi, Thymoquinone prevents endoplasmic reticulum stress and mitochondria-induced apoptosis in a rat model of partial hepatic warm ischemia reperfusion, *Biomed. Pharmacother.*, 2017, **94**, 964–973, DOI: 10.1016/j.biopha.2017.08.018.

40 E. Kaymak, A. T. Akin, E. Öztürk, D. Karabulut, N. Kuloğlu and B. Yakan, Thymoquinone has a neuroprotective effect against inflammation, oxidative stress, and endoplasmic reticulum stress in the brain cortex, medulla, and hippocampus due to doxorubicin, *J. Biochem. Mol. Toxicol.*, 2021, **35**(11), e22888, DOI: 10.1002/jbt.22888.

41 E. Kaymak, E. Öztürk, A. T. Akİn, D. Karabulut and B. Yakan, Thymoquinone alleviates doxorubicin induced acute kidney injury by decreasing endoplasmic reticulum stress, inflammation and apoptosis, *Biotech. Histochem.*, 2022, **97**(8), 622–634, DOI: 10.1080/10520295.2022.2111465.

42 C. Christowitz, T. Davis, A. Isaacs, G. van Niekerk, S. Hattingh and A. M. Engelbrecht, Mechanisms of doxorubicin-induced drug resistance and drug resistant tumour growth in a murine breast tumour model, *BMC Cancer*, 2019, **19**(1), 757, DOI: 10.1186/s12885-019-5939-z.

43 S. Mirzaei, M. H. Gholami, F. Hashemi, A. Zabolian, M. V. Farahani, K. Hushmandi, A. Zarrabi, A. Goldman, M. Ashrafizadeh and G. Orive, Advances in understanding the role of P-gp in doxorubicin resistance: Molecular pathways, therapeutic strategies, and prospects, *Drug Discov. Today*, 2022, **27**(2), 436–455, DOI: 10.1016/j.drudis.2021.09.020.